Universiteit Utrecht

*-Master of Science Thesis-*

# Reproducible benchmark models of asteroid/comet objects for radar modeling and imaging

Anastasios Fyssas

Defended on March 5, 2018

*Supervisors:* *Assist. Prof. Ivan Pires de Vasconcelos*
*Assist. Prof. Inge Loes ten Kate*

**Utrecht University**
**Faculty of Geosciences**
**February 2018**

# REPRODUCIBLE BENCHMARK MODELS OF ASTEROID/COMET OBJECTS FOR RADAR MODELING AND IMAGING

By
Anastasios Fyssas

# ABSTRACT

After reviewing the existing Planetary Science literature for suitable asteroids of various size, shape, and composition, asteroids 25143 Itokawa, 433 Eros, and 511 Davida were selected, along with comet 67P/Churyumov – Gerasimenko to be numerically modeled using MATLAB for EM wave propagation. Essential elements were captured (formation, composition, differentiation, etc.), based on their current evolutionary models, covering different scenarios of rubble pile structure, cometary contact binary, and partial differentiation. Geometric information for these bodies was found and used from online databases (DAMIT, NASA) with the objective of generating reproducible numerical models of the internal structure of the selected bodies. The results are presented and discussed, while more internal structure scenarios are proposed for future modeling.

TABLE OF CONTENTS

LIST OF FIGURES

LIST OF TABLES

# CHAPTER 1

# INTRODUCTION

Over the last 20 years, there have been numerous missions on asteroids and comets (NEAR shoemaker mission, Rosetta, etc.) that supplied the scientific community with valuable data related to topography, composition, and physical parameters. These findings lead to a better understanding of their evolution as well as the history of the early solar system. However, their internal structure remains elusive with no direct observations, while scientists must rely on remote sensing observations, and formation/evolution modeling to speculate on the nature of asteroid's internal structures. Moreover, because of the likely abundance of valuable materials that asteroids contain, they also present potentially highly valuable economic prospects in the context of space mineral exploration.

One potentially effective way to image deep asteroid interiors is by using radar systems that perform reflection imaging of internal contrasts, instead of data transmitted through the object (Sava et al. 2015; Grimm et al. 2015; Safaeinili et al. 2010; Herique et al. 2017). Sava et al. in 2015, used a scaled version of 433 Eros to illustrate this methodology (fig. 1). The model contains two different materials of rock and regolith which is representative for a rubble pile structure. The current work is focused on taking such models a step further by creating similar benchmark

numerical models that also take internal structure scenarios such as rubble pile structures with different compositions, partial differentiation, and latest mission results under consideration to produce more accurate and realistic models of different asteroid bodies.

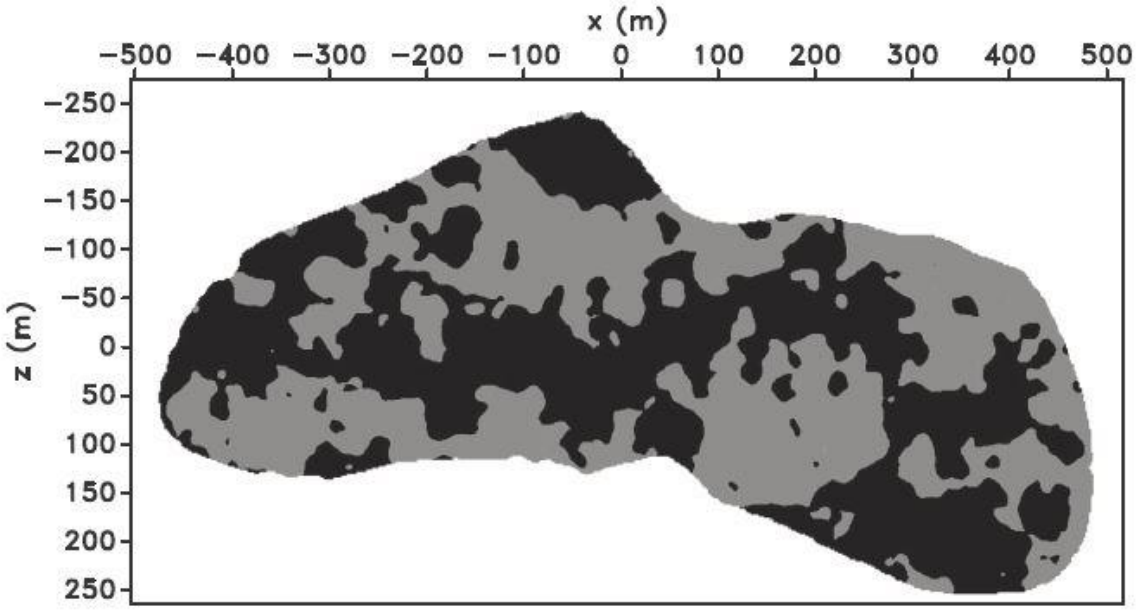


*Fig. 1. 433 Eros model representing two different materials: rock (black) and regolith (grey), Sava et al. 2015*

# CHAPTER 2

# ASTEROID CLASSIFICATION

The criteria with which the following asteroids were chosen were size, composition and targets of completed space missions, considering only chondritic bodies. Achondrites are linked to differentiation processes that suggest the formation of metallic cores in large asteroids. These formations would greatly attenuate radio waves thus being of lesser interest for radar imaging purposes. Before each individual asteroid is examined, it is necessary to review the various chondrite classification types and their differences.

## Classification system

Meteorites are divided into three main categories depending on the percentages of silicate/iron content.

- Stony meteorites (composed mostly of “stony” siliceous materials, S-type asteroids)
- Stony-Iron (mixture of siliceous/metallic content)
- Iron (mostly metallic material)

The Stony meteorites group is a vast one that contains both chondrites and achondrites. The main difference between chondrites and achondrites, is that the latter underwent melting and recrystallization and as a result they lack chondrules (small grains produced by molten material). Chondrites are stony meteorites that have not been altered by differentiation of the body they originated from (the parent body). They are divided into 3 distinct classes based on their mineralogy, oxygen isotopic compositions, and bulk chemical composition. Figure 2 shows an overview of the classification system.

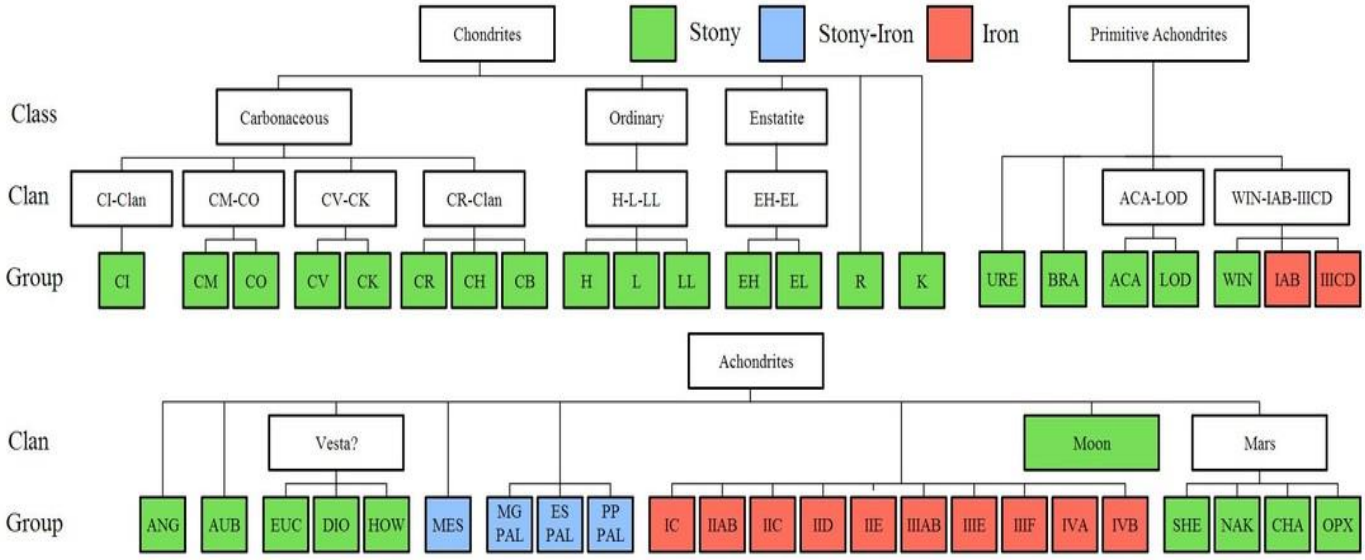


*Fig. 2. Meteorite classification (Weisberg et al. 2006)*

Carbonaceous Chondrites (especially the CI – CM groups) are undifferentiated meteorites that contain water and large amounts of carbon and organic compounds (Ehrenfreund et al. 2001). Due to the extensive aqueous alterations, their composition is mostly made up of hydrous phyllosilicates and olivine crystals and they have been linked with the most primitive nebular compositions (McSween 1977). Although aqueous alterations are dominant, thermal metamorphism is thought to be absent.

Ordinary Chondrites (OCs), on the other hand, can experience thermal metamorphism with temperatures above 500 $^{o}$C on the parent bodies but do not contain any water or organic compounds. The most usual composition includes olivine, pyroxene, plagioclase, and metal content depending on the specific group (Weisberg et al. 2006). OCs are divided into three groups: H group has high total Fe contents (FeO as Fa and metallic Fe), L group has low total Fe, and LL group has the lowest metallic Fe as well as low total Fe.

Petrologic types

Asteroids can also get affected by secondary processes of thermal metamorphism and aqueous alteration. Depending on the degree of these processes,

Van Schmus and Wood in 1967 created a scheme that assigns petrologic types 1-6 to different meteorite classes (fig. 3).

- **Type 1** refers mostly to the CI group where due to the extensive aqueous alteration, there is lack of chondrules, and most of the olivine and pyroxene have changed to hydrous phases.
- **Type 2** is a "middle ground" between type 1 and type 3. In this type, aqueous alteration is still present, however there are still percentages of unaltered chondrules, olivine and pyroxene.
- **Type 3** is considered the pristine condition for all groups, having similar composition with the parent body.
- **Types 4,5,6** show increasing degrees of thermal metamorphism (>400 $^{o}$C). As the temperature rises, the matrix gets recrystallized and coarser, chondrules become indistinct from the rest of the material, and feldspar starts to form.

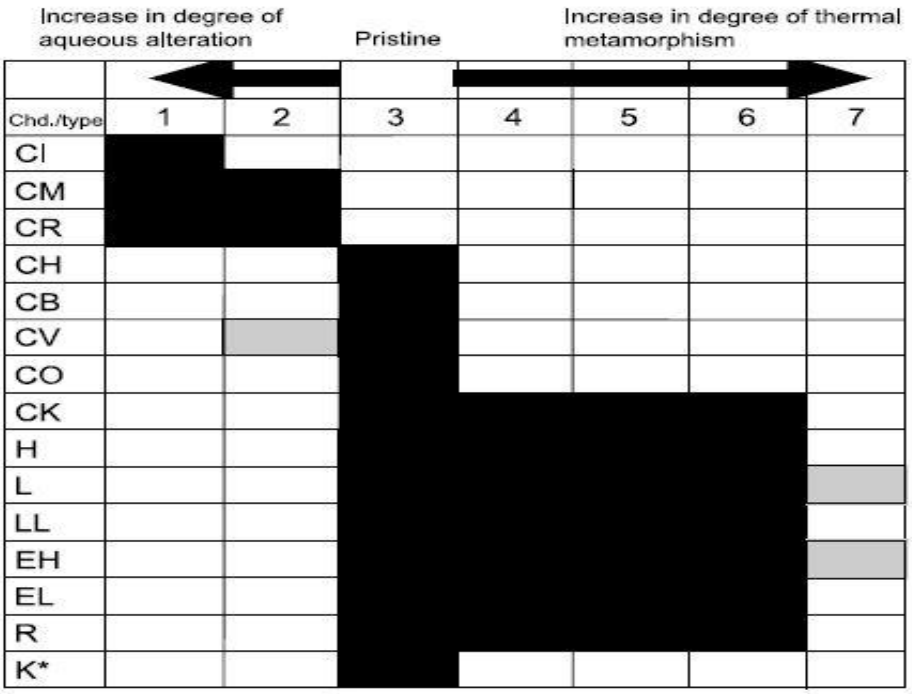


*Fig. 3. Petrologic types 1-6 (Weisberg et al. 2006)*

Type 7 is a transitional stage between chondrites and primitive achondrites, where partial melting begins to take place.

## 2.1 25143 Itokawa

Itokawa (fig. 4) is a small near-Earth object visited by the Hayabusa spacecraft in 2005. It has a mean diameter of 0.33km and is classified as an S-type asteroid with an LL4-LL6 (OC) composition mostly containing pyroxene and olivine (Abell et al. 2006; Nakamura et al. 2011). Its internal structure is unknown, and generates debate in the scientific community, with the most common model being a rubble pile

(Fujiwara et al. 2006). However, due to the different densities observed between the body and the head of the asteroid, it could also be possible that Itokawa is a contact binary, created by two separate bodies (Lowry et al. 2014).

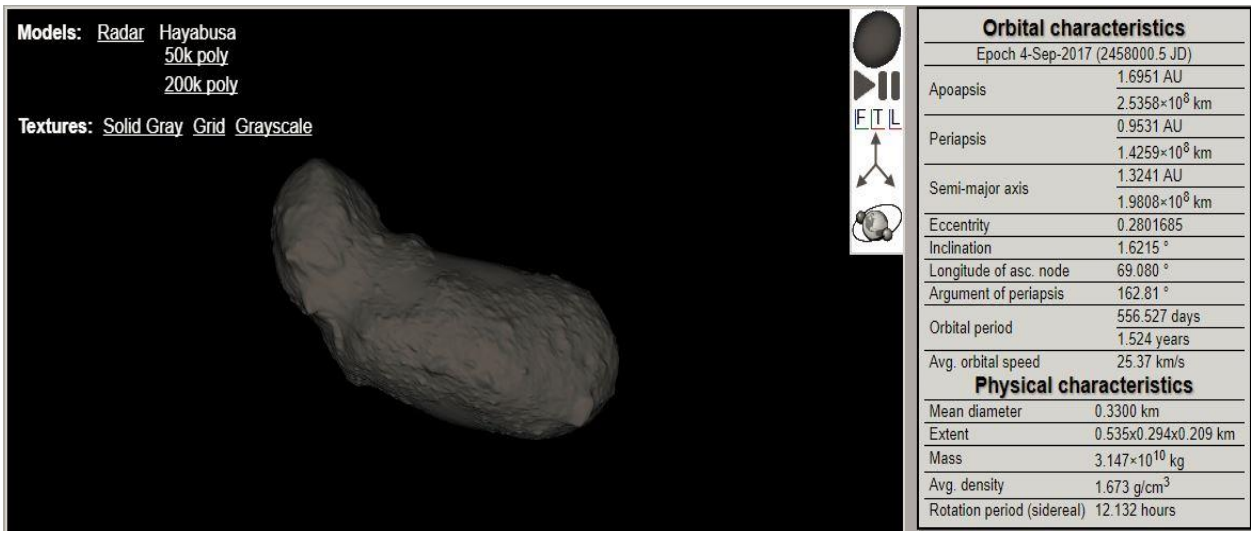


| Orbital characteristics | |
|---|---|
| Epoch 4-Sep-2017 (2458000.5 JD) | |
| Apoapsis | 1.6951 AU |
| | $2.5358\times10^{8}$ km |
| Periapsis | 0.9531 AU |
| | $1.4259\times10^{8}$ km |
| Semi-major axis | 1.3241 AU |
| | $1.9808\times10^{8}$ km |
| Eccentrity | 0.2801685 |
| Inclination | 1.6215 ° |
| Longitude of asc. node | 69.080 ° |
| Argument of periapsis | 162.81 ° |
| Orbital period | 556.527 days |
| | 1.524 years |
| Avg. orbital speed | 25.37 km/s |
| **Physical characteristics** | |
| Mean diameter | 0.3300 km |
| Extent | 0.535x0.294x0.209 km |
| Mass | $3.147\times10^{10}$ kg |
| Avg. density | 1.673 g/cm$^3$ |
| Rotation period (sidereal) | 12.132 hours |

*Fig. 4. 25143 Itokawa 3D shape (3D asteroid catalogue)*

## 2.2 433 Eros

One of the most studied asteroids, Eros (fig. 5) is the second largest near-Earth object, with a mean diameter of 16,84km, which was visited by the NEAR Shoemaker spacecraft that orbited Eros between 2000 – 2001 providing much data through remote sensing. It is also classified as an S-type asteroid with mineralogy similar to that of an ordinary chondrite (Foley et al. 2006). Much like Itokawa, Eros

is commonly described as a rubble pile. On the other hand, some studies suggest that its macroporosity and density are lower than those expected in a rubble pile structure, with an addition of a significant degree of internal strength, suggesting that its internal structure to be that of a heavily fractured asteroid rather than a rubble pile (Andrew F. Cheng 2003; Wilkison et al. 2002).


*Fig. 5. 433 Eros 3D shape (3D asteroid catalogue)*

## 2.3 511 Davida

Davida (fig. 6) is the Solar system's 7$^{th}$ largest asteroid and holds a mining value of more than $100tn (Cookson 2017). It has a mean diameter of 290 ±20km and is classified as a C-type asteroid (CI – CM) (Reddy et al. 2015) with a

carbonaceous chondrite composition. Little is known about its internal structure.


*Fig. 6. 511 Davida 3D shape (3D asteroid catalogue)*

## 2.4 67P/Churyumov – Gerasimenko

Gerasimenko (fig. 7) is a famous comet visited by the Rosetta mission (ESA) in 2014. Its main components are ice – dust with a crust rich in polyaromatic organic solids mixed with sulfides and Fe – Ni alloy (Quirico et al. 2015). The comet's characteristic double lobed form led to the argument of whether this is due to erosion in the 'neck' area, or whether the whole comet is a contact binary with two separate lobes that merged together (Sierks et al. 2015). After the Rosetta mission observations, a new study concluded that the lobes, although quite similar, formed separately with a similar stratified accretion, and merged under a low speed collision (Massironi et al. 2015).

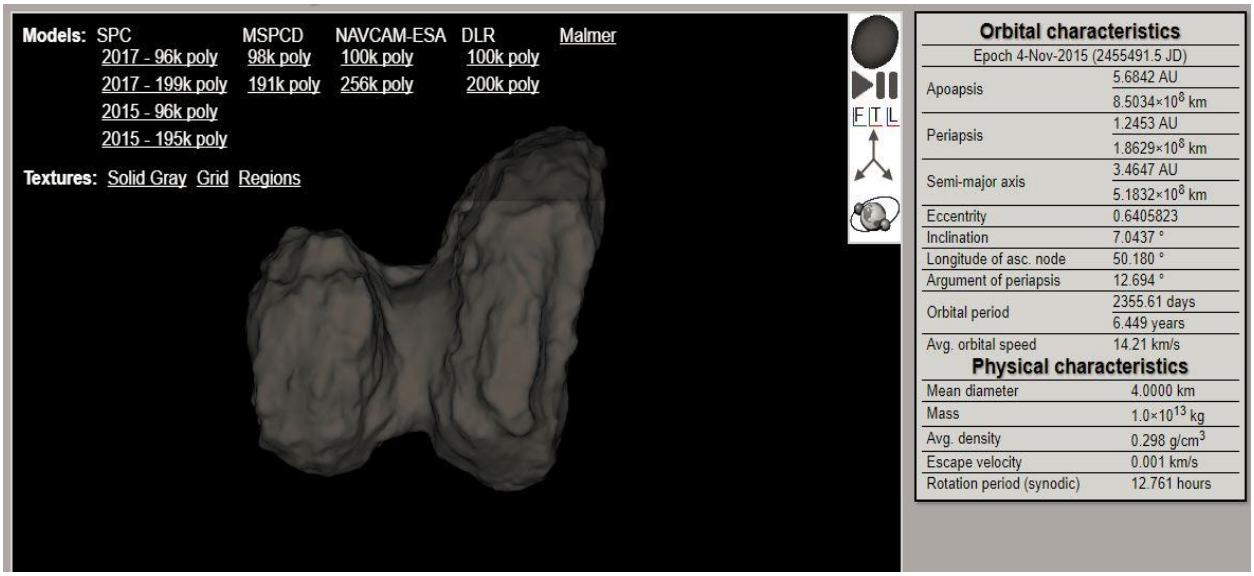


*Fig. 7. 67P/Churyumov – Gerasimenko 3D shape (3D asteroid catalogue)*

# CHAPTER 3

# ASTEROID ACCRETION SCENARIOS

If specific physical and compositional assumptions about the parent bodies are made then, after gravitational breakup and re-accretion, the resulting asteroid bodies will also share these common characteristics with the original parent bodies. Thus, in order to create realistic numerical models of asteroid interior, it would seem logical to first consider the possible features of the parent bodies of these asteroids, and what could remain in the interior after the assembly of the latter.

## 3.1 RUBBLE PILE SCENARIOS

As described in sections 2.1 and 2.2, Eros and Itokawa are considered rubble piles with an interior made up of regolith and rock. However, Wilkison et al. in 2001, presented various parent body formation models applicable to 433 Eros (fig. 8). One interesting scenario, derived from these models, could be the creation of a parent body where successive layers of petrological types 3-6 populate the interior, created by thermal metamorphism, as a result of external or internal heating (fig. 8-B). After a collisional breakup and a gravitational reassembly, Eros could have been created as a rubble pile with an interior made of regolith and rock fragments originating from the different layers of the parent body (fig. 9). The same scenario is also applicable to 25143 Itokawa, as Nakamura et al. (2011) and Abell et al. (2006) identified dust particles of petrologic types LL4-6 concluding that the parent body of Itokawa must had experienced intense thermal metamorphism before being disaggregated and reaccreted into smaller bodies like Itokawa. Both models of rubble pile structure (regolith/rock, regolith/LL4-6 rock fragments) will be explored.

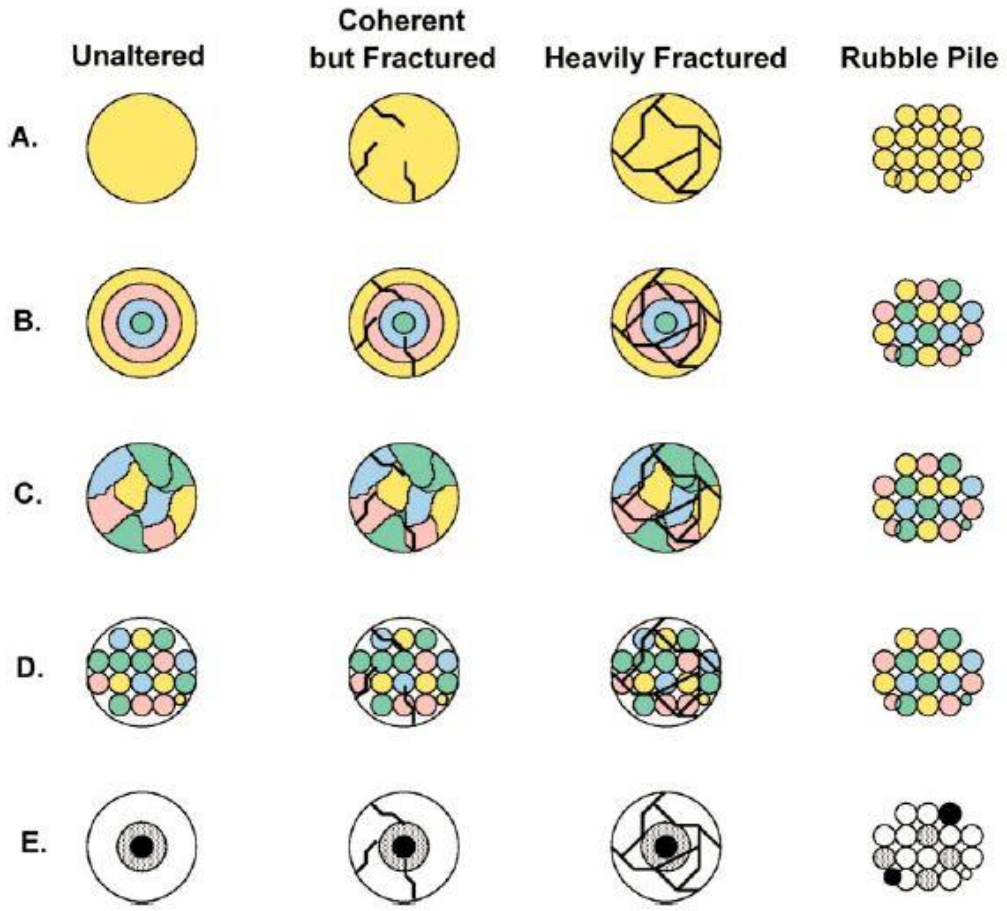


*Fig. 8. Parent body formation models for 433 Eros, Wilkison et al. (2001).*
*A. The undifferentiated model, after Wetherill and Chapman (1988).*
*B. The onion shell model, after Miyamoto et al. (1981).*
*C. The heterogeneously heated model, as described in McCoy et al. (1990).*
*D. The metamorphosed planetesimal model, after Scott and Rajan (1981).*
*E. The differentiated model, after Wetherill and Chapman (1988).*

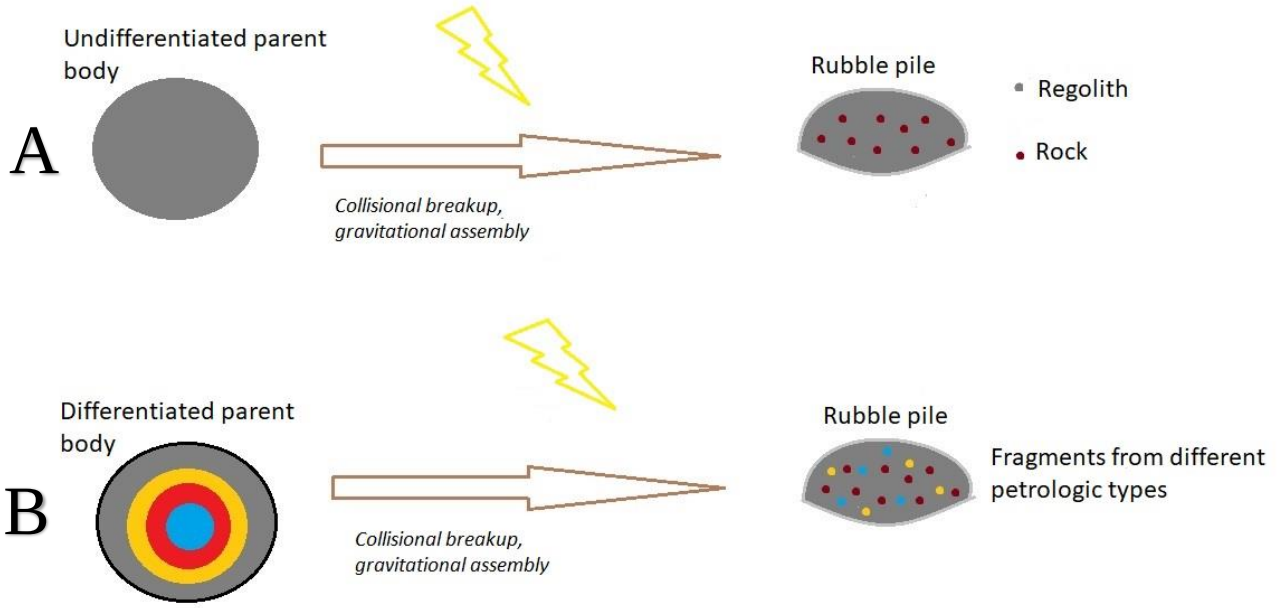


*Fig. 9. Breakup and re-assembly of different parent bodies*
*A. Undifferentiated parent body resulting in regolith/rock rubble piles*
*B. Differentiated parent body resulting in regolith/rock of multiple petrologic types rubble piles*

## 3.2 PARTIALLY DIFFERENTIATED DAVIDA SCENARIO

511 Davida is a large asteroid where, because of its size, it would not seem realistic to use the previous scenarios of accretion from an older parent body. Similar asteroids of the same type of different sizes (C-type, 253 Mathilde – 52,8 km, 1 Ceres – 939.4km mean diameters), have quite different internal structures. Mathilde is believed to be a rubble pile because of its low bulk density and a porosity larger than 50% (Herique et al. 2017), while 1 Ceres is a differentiated dwarf planet. Although Davida is not large enough to have been fully differentiated, a middle

ground is chosen for this current study. Gaffey et al. (1993) present the generalized properties of partially differentiated bodies at different levels of degree of partial melting for various chondritic types. A C-type body (CV – CO types) that reached low degrees of partial differentiation, would develop a thin basaltic crust with intrusions into shallow olivine crustal layers as well as an interior made up of olivine – FeS/FeNi interior (mean ratio Ol – FeS, FeNi 10:1) but no presence of metallic core. This could also be applicable to Davida, as the main difference between CI – CM types and CO – CV types is the aqueous alteration because of the presence of water on, at least, the surface. For this study, both rubble pile and partially differentiated options will be explored.

## 3.3 GERASIMENKO MODEL

As discussed in section 2.4, Massironi et al. (2015) concluded that Gerasimenko is made up of two distinct objects that formed with a stratified accretion (similar to 9P/Tempel 1) before merging into a single body. Following this study, the adopted model will include an external layer representing a loose regolith material covering the earlier formed internal nuclei, and two internal areas representing the contact nuclei themselves. The “stratified accretion” is left out of

the scope of this study, as it is a part of the "layered pile" model of 9P/Tempel 1 suggested by Belton et al. 2006.

# CHAPTER 4

# RESULTS

## 4.1 METHODOLOGY

In this section the general methodology and workflow followed will be presented.

3D shape files

The starting point of this work is the 3D shape files of the chosen bodies that were downloaded and imported in MATLAB (point cloud format) by the following online databases:

- DAMIT database (Database of Asteroid Models from Inversion Techniques, Astronomical Institute of the Charles University in Prague, Czech Republic)
- JPL asteroid RADAR research database, NASA
- 3D asteroid catalogue by Greg Frieger ( https://space.frieger.com/asteroids/ )

All shape files, apart from Davida, are highly detailed shape models that have their axis dimensions in kilometers, so no conversion was necessary. The Davida shape model is derived from light curve inversions with arbitrary units that were converted into kilometers. All 3D point cloud files were converted into 3D arrays and reduced to 2D afterwards choosing a “slice” from the middle of each body. An example of this process is given in figure 10.

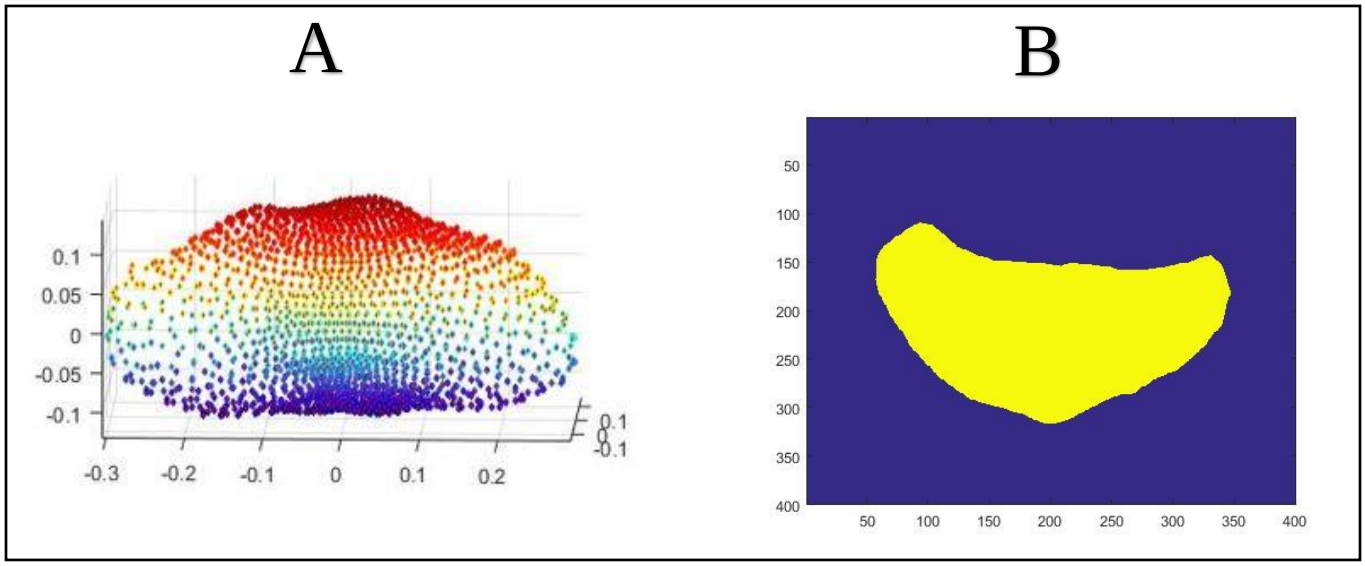


*Fig. 10. A. Itokawa 3D pointcloud file*
*B. Resulting Itokawa MATLAB 2D array*
*(size 400x400)*

Spatial Process Simulation (random fields)

All 2D arrays were populated with stationary isotropic/non-isotropic Gaussian fields generated via circular embedding, as described by Dirk P. Kroese and Zdravko I. Botev in the book "Stochastic geometry, Spatial Statistics and random fields" (Springer 2015). In the cases of Eros and Itokawa, the fields were clipped in order to produce randomly distributed areas with an equal index number (fig. 11, B) to represent defined areas that separate different material (rock/regolith). In the cases of Davida and Gerasimenko, the random fields were left unchanged to represent a variation in composition rather than distinct material boundaries (fig. 11, A) (e.g. Gerasimenko - ice/dust ratio).

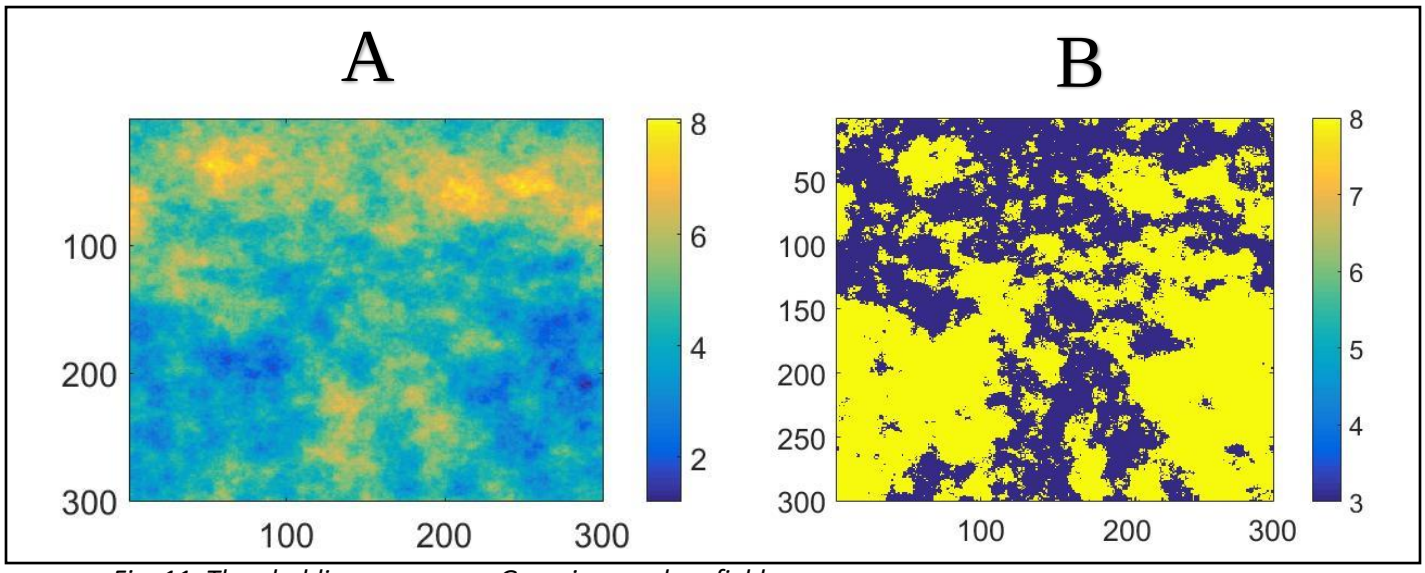


*Fig. 11. Thresholding process on Gaussian random field*
*A. Original Gaussian field*
*B. Gaussian field after thresholding with only two index numbers: 3 and 8*

## 4.2 NUMERICAL MODELLING RESULTS

### 4.2.1 CLASSIC RUBBLE PILE MODELS

Figures 12, 13 and 14 show the results of asteroids Davida, Eros and Itokawa respectively as classic rubble piles populated by two distinct colors that represent different phases of material. Index number 3 is assigned as the regolith and index number 8 as rock fragments between the regolith material.

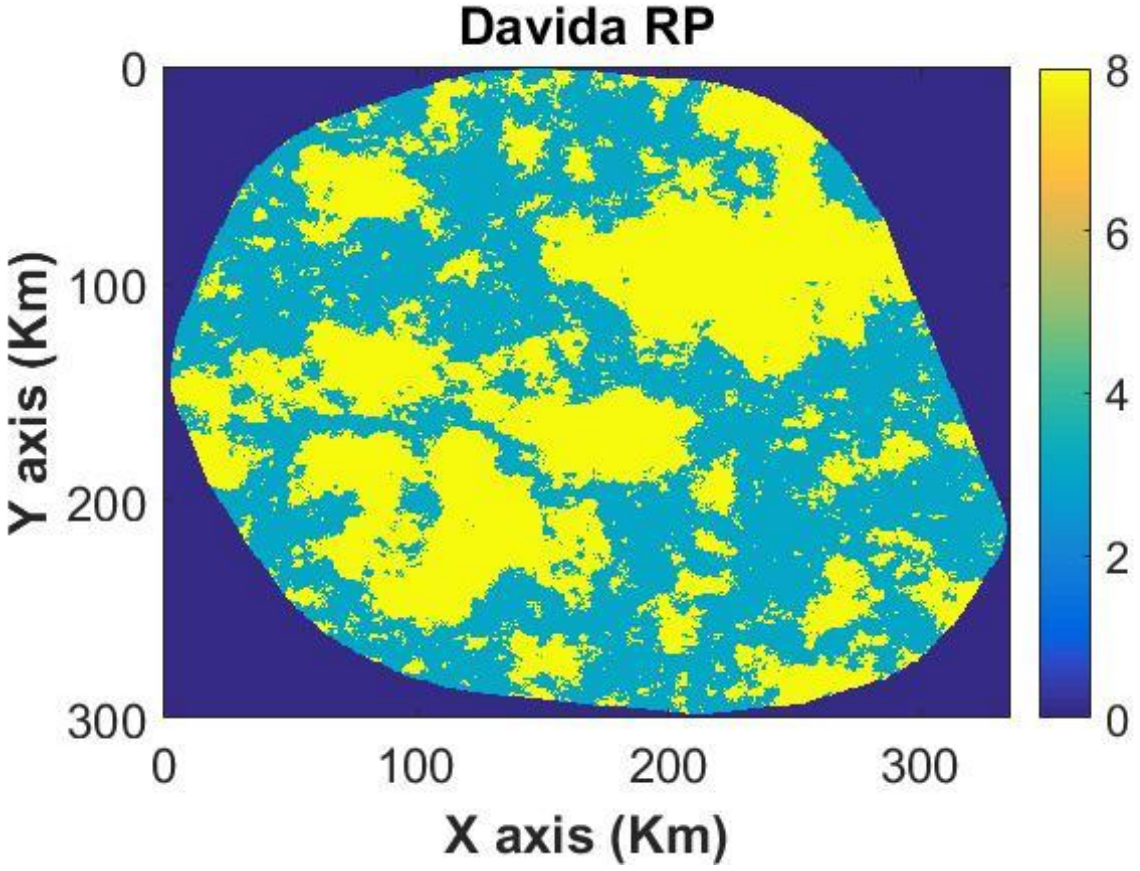


*Fig. 12. Davida rubble pile model (regolith/rock)*
*index number 3 – regolith*
*index number 8 – rock*

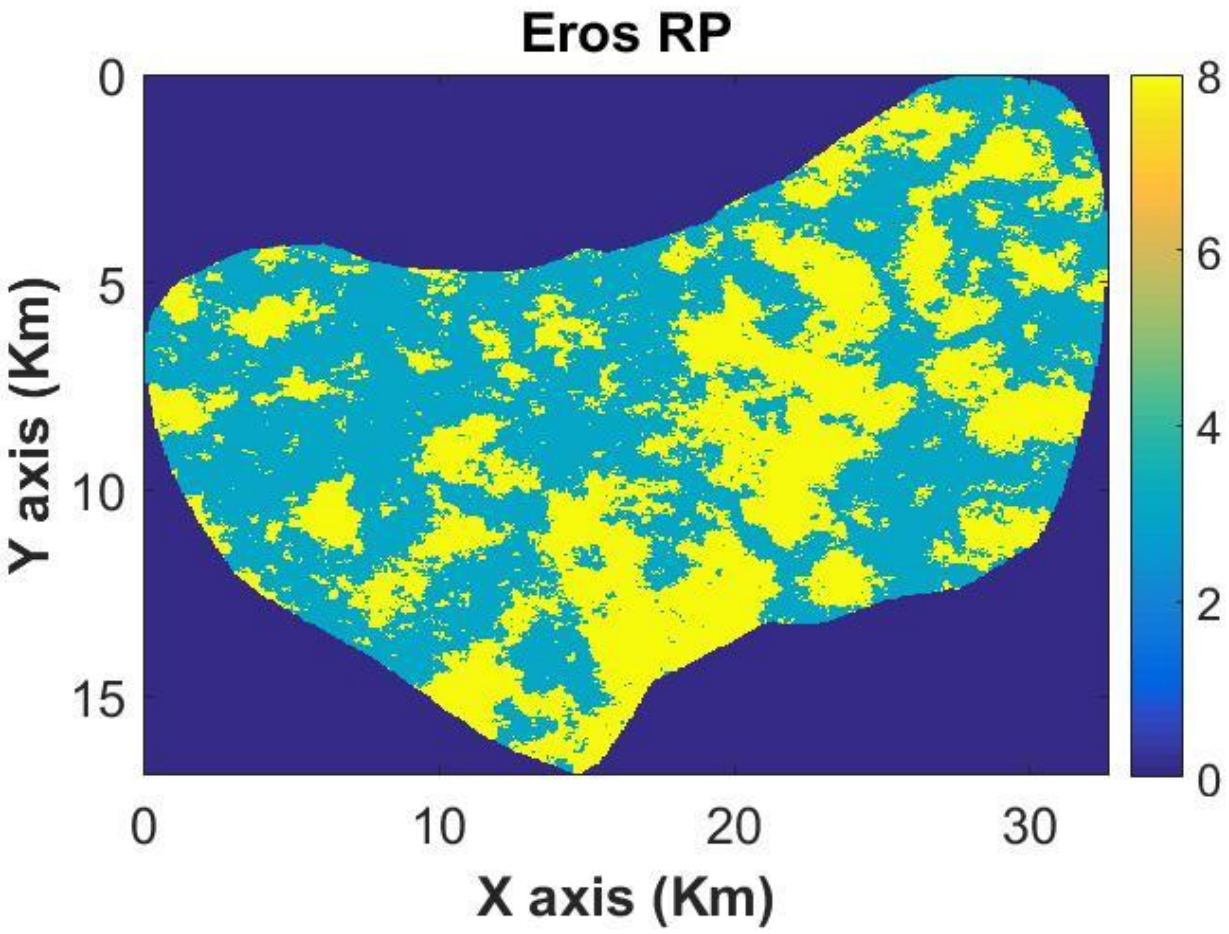


*Fig. 13. Eros rubble pile model (regolith/rock)*
*index number 3 – regolith*
*index number 8 – rock*

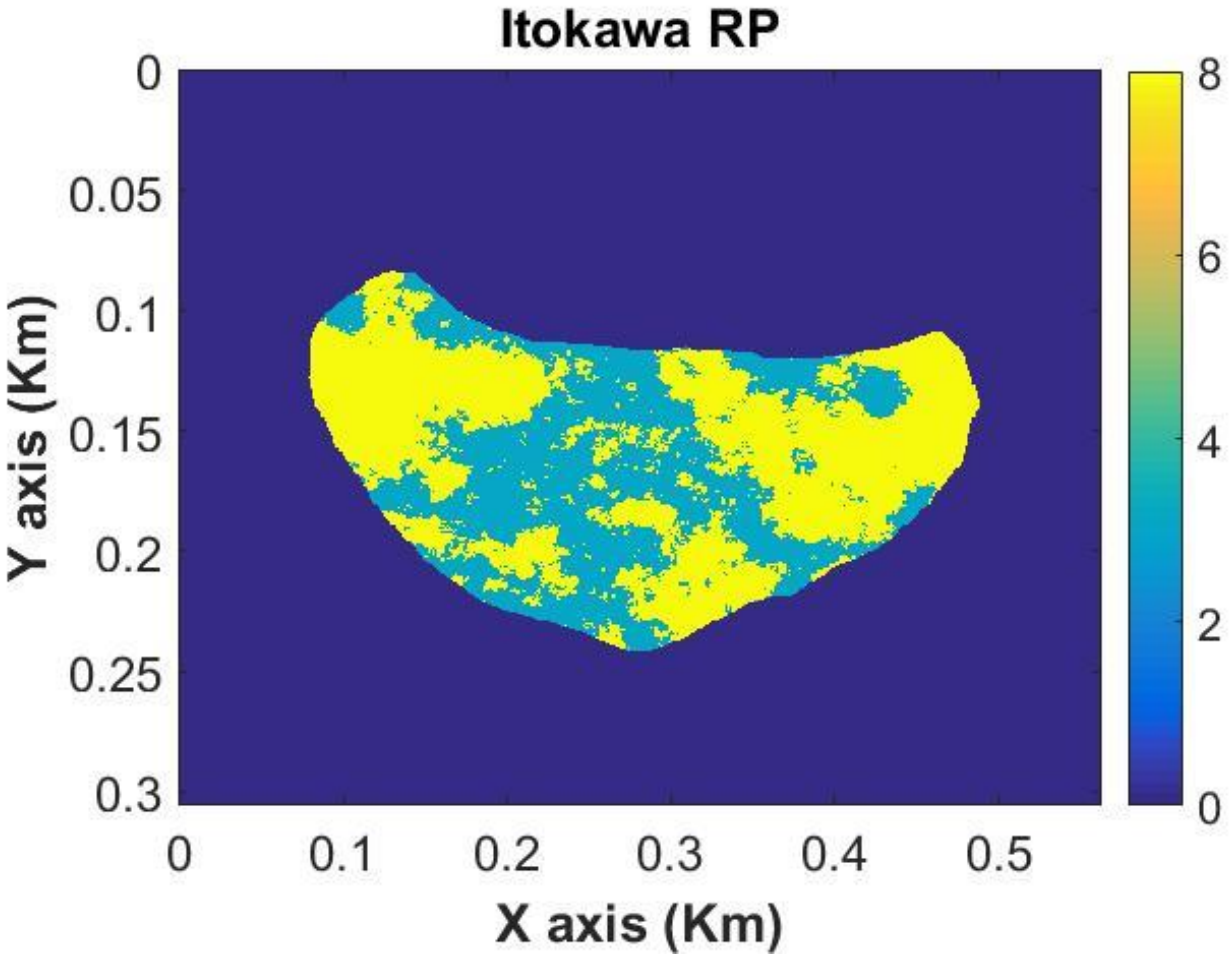


*Fig. 14. Itokawa rubble pile model*
*index number 3 – regolith*
*index number 8 – rock*

### 4.2.2 LL4-6 RUBBLE PILES

Because we want to produce an interior with rock fragments of petrologic types 4 to 6, along with possibly unaltered fragments of type 3, instead of separating the random field into two areas, we now threshold it accordingly to produce five distinct areas of index numbers. Figures 15, 16 show the results obtained through this process for asteroids Itokawa and Eros respectively. In this study, no particular assumption was made for the percentages of each petrologic type with respect to the whole volume of the asteroids. However, it would seem logical to assume that because of the different petrologic types that come from different parts of the parent asteroid, the heavily altered inner layers of the parent body asteroid would appear in smaller percentages in reaccreted bodies like Eros and Itokawa.

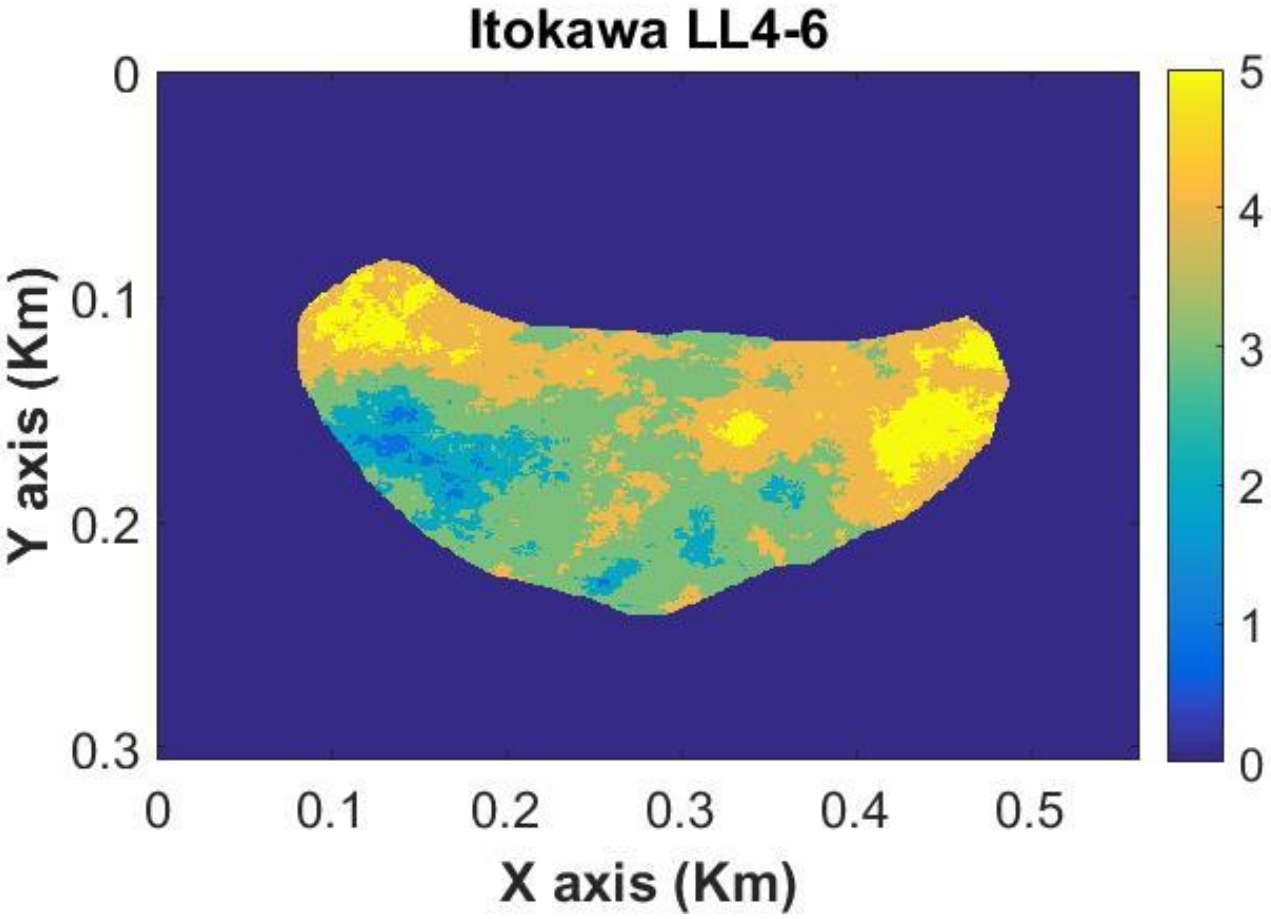


*Fig. 15. Itokawa LL4-6 rubble pile*
*index number 1 – small percentage of LL6 fragments*
*index number 2 – LL5 fragments*
*index number 3 – regolith*
*index number 4 – LL4 fragments*
*index number 5 – LL3 (unaltered) fragments*

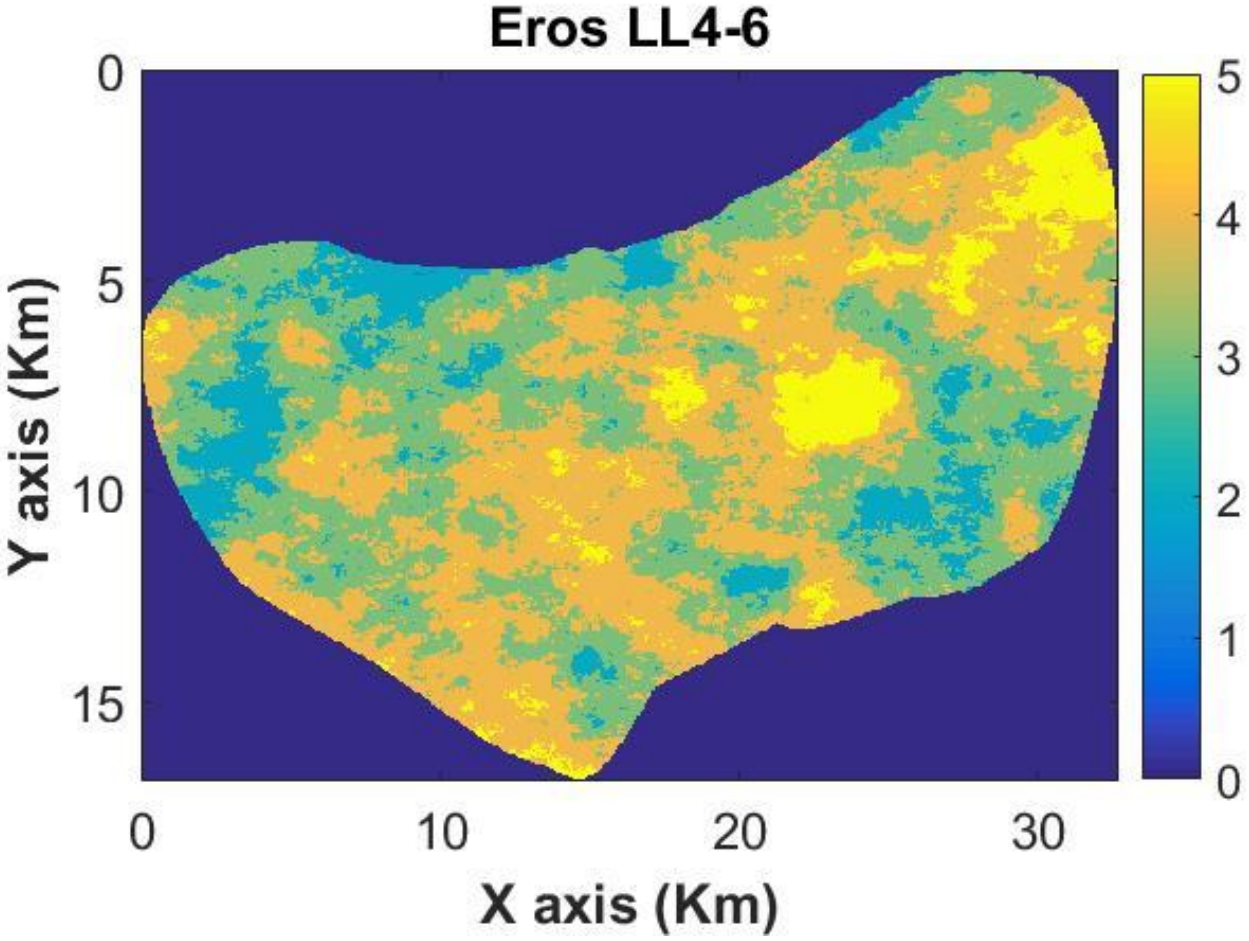


*Fig. 16. Eros LL4-6 rubble pile*
*index number 1 – small percentage of LL6 fragments*
*index number 2 – LL5 fragments*
*index number 3 – regolith*
*index number 4 – LL4 fragments*
*index number 5 – LL3 (unaltered) fragments*

### 4.2.3 GERASIMENKO NUMERICAL MODEL

In figure 17 the model of Gerasimenko is displayed. As discussed in sections 3.4 and 4.1, the interior (fig. 17, A) is filled with an isotropic gaussian random field that demonstrates the variation between ice and dust composition. The outer layer (fig. 17, B) is made up of an anisotropic gaussian random field that corresponds to a looser kind of material that covers the primordial nuclei and could also be affected by space weathering. Finally, according to Sierks et al. 2015, there should be a structural difference between the neck area (fig.17, C) and the rest of the comet,

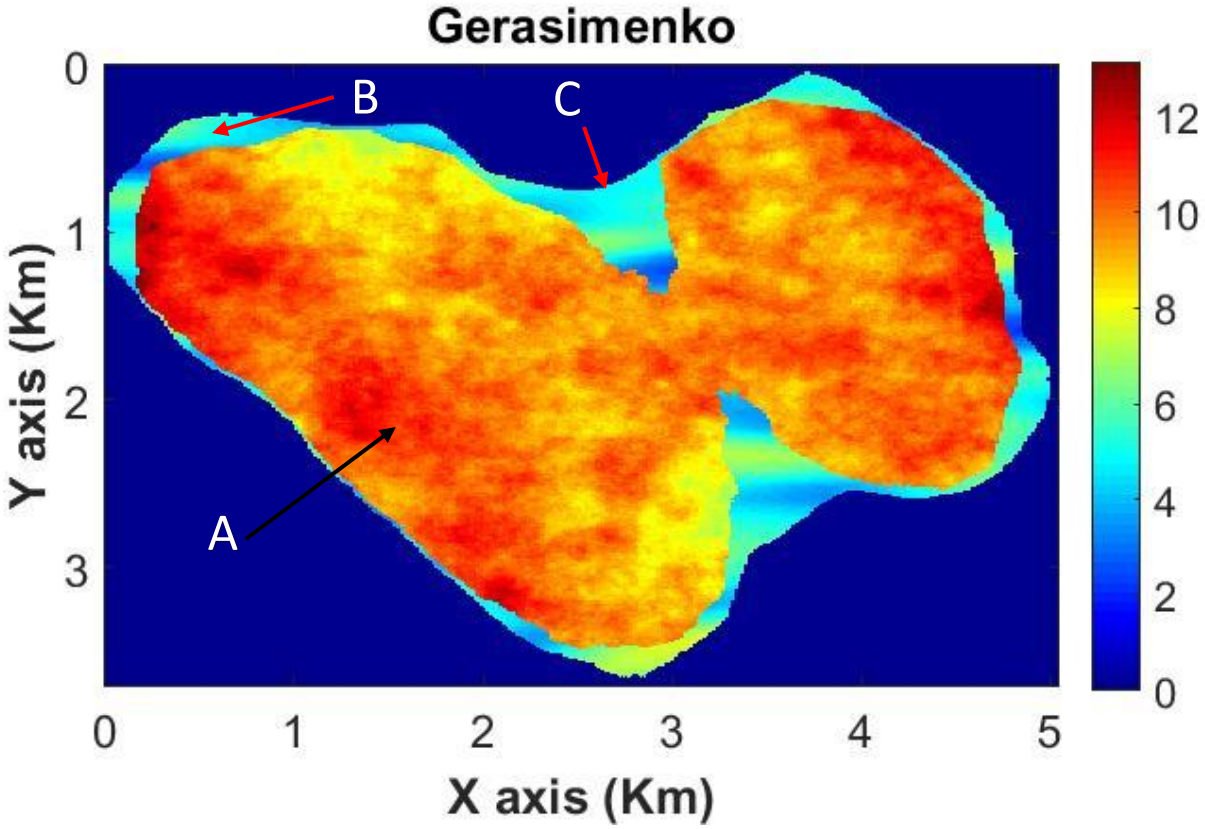


*Fig. 17. Gerasimenko model*

*A. Inner random field – collision nuclei made up of ice/dust*

*B. Outer random field – loose material covering the inner nuclei*

*C. Neck area*

which was applied here, creating a larger depth of the outer loose material in the neck area.

### 4.2.4 DAVIDA DIFFERENTIATED NUMERICAL MODEL

For the realization of the scenario presented in section 3.3, four layers were created inside Davida. The random field that was applied was scaled, with different percentages for each layer to represent the change in variation intensity from the inner layers to the outer ones as seen in table 1.

Table 1

Differential scaling for each individual Davida layer.

| Davida individual layers | Scaling of original field | Variation range |
|---|---|---|
| Layer 1 – inner layer | 1% | 0.6 – 0.9 |
| Layer 2 | 5% | 2.5 – 4.5 |
| Layer 3 | 15% | 7.5 - 12 |
| Layer 4 – outer layer | 85% | 40 - 60 |

This was done in order to show the transition difference of the homogeneity between the inner and the outer layers. In figure 18 the complete model is given, but for visualisation purposes all individual layers are presented in Figure 19.

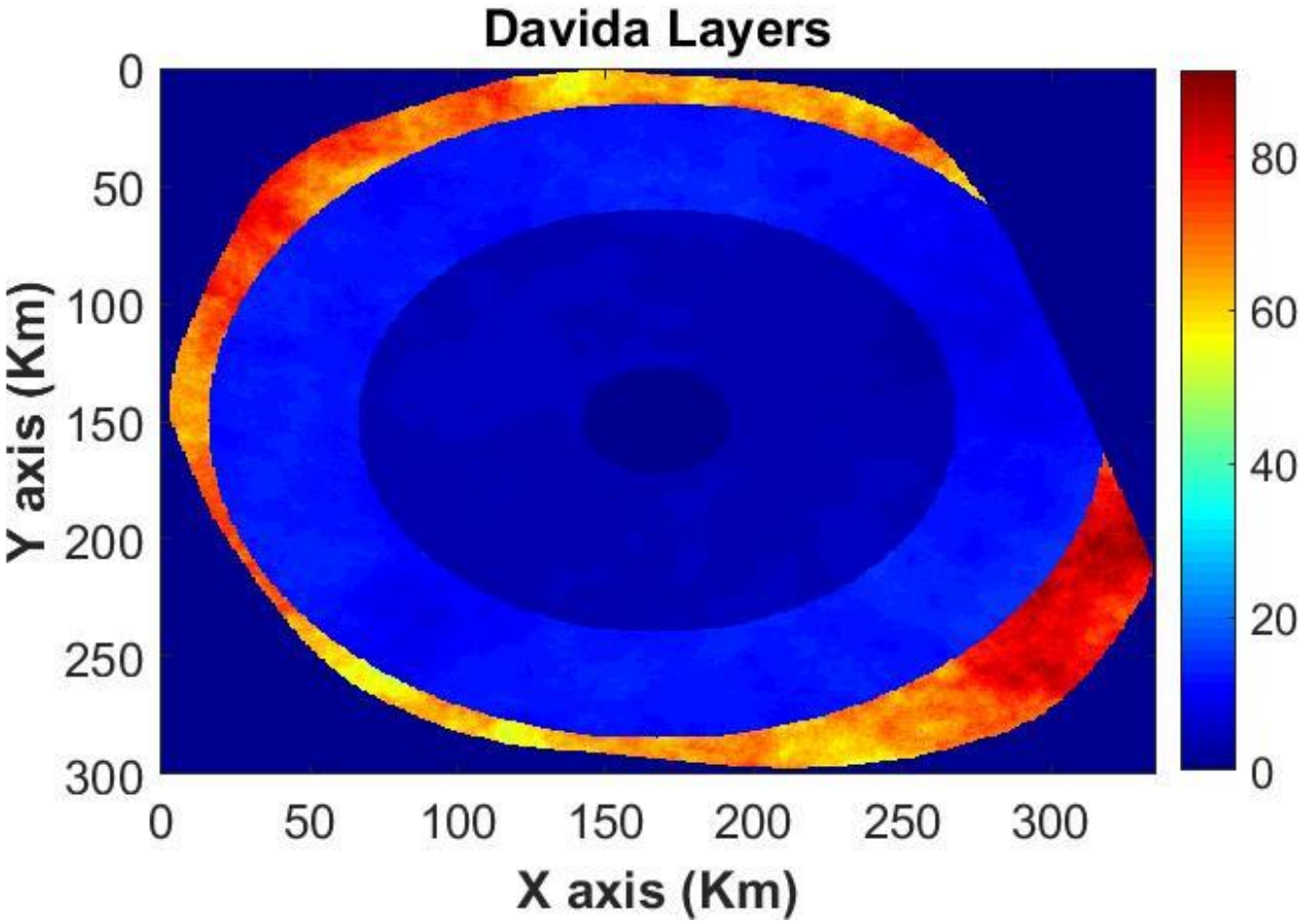


*Fig. 18. Davida full layered model*

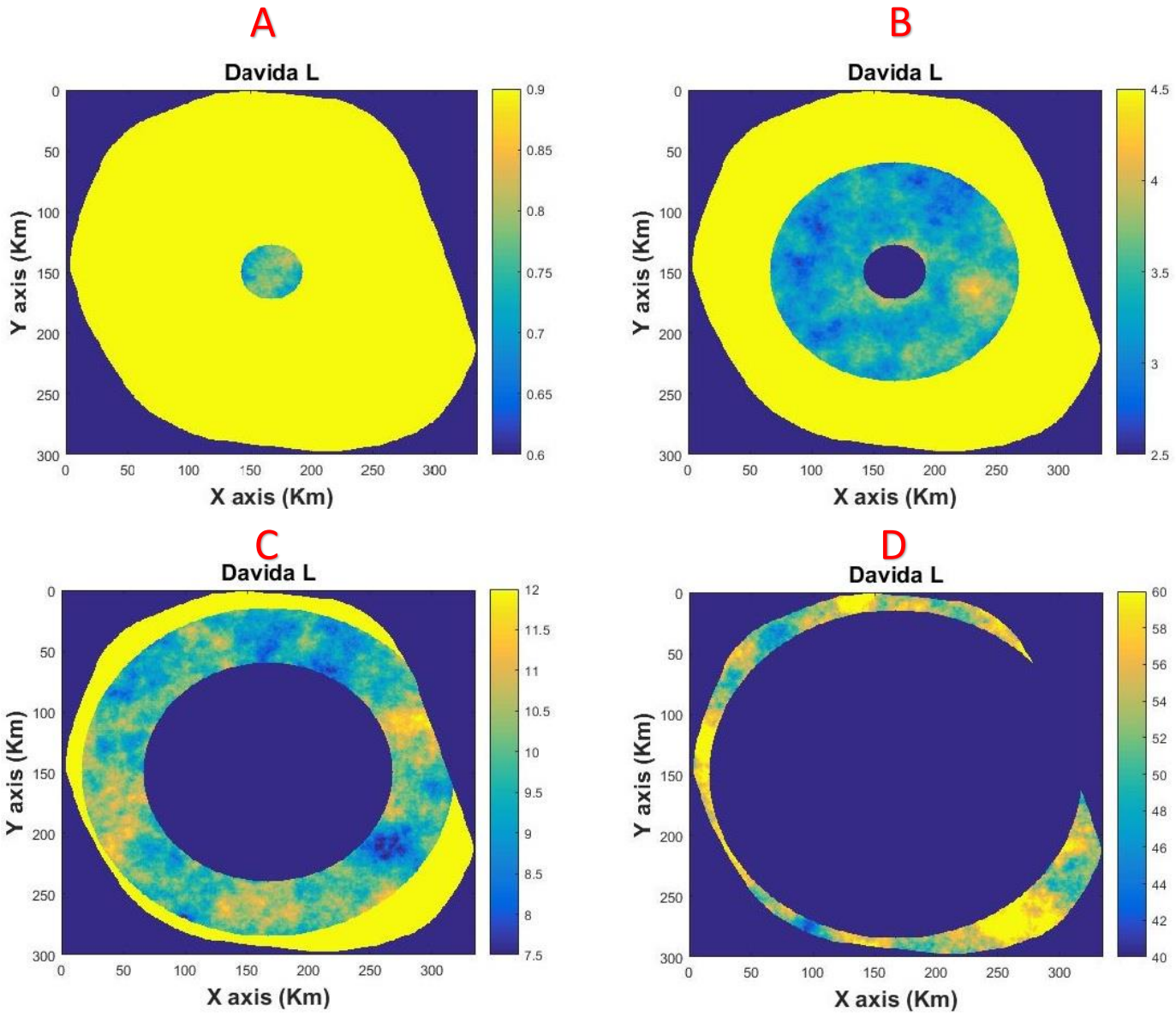


*Fig. 19. Davida individual scaled layers*

*A. Layer 1 inner layer – 1% scaling*

*B. Layer 2 – 5% scaling*

*C. Layer 3 – 15% scaling*

*D. Layer 4 outer layer – 85% scaling*

# CHAPTER 5

# DISCUSSION AND CONCLUSION

After exploring the available literature for the structure and composition of asteroids Eros, Itokawa, Davida and comet Gerasimenko, various scenarios of their internal structure were created. Using the available shape files of these asteroids in MATLAB, reproducible numerical models that describe each scenario were produced.

In order to use the above numerical models in radar imaging, the first step is to convert the arbitrary numbers of the random fields into numbers that represent a physical parameter. For EM wave propagation in asteroids, the most important parameter that controls the radar response is the complex dielectric permittivity (ε). It is composed of two parts; the real part ε' is connected with the EM wave velocity while the imaginary part ε'' relates to the wave absorption, usually represented as the loss tangent tanδ (Herique et al. 2017). To achieve this conversion, the theorized mineralogy and material phases/components of each asteroid must be cross referenced with permittivity constrains gained from laboratory measurements of meteorite samples, surface observations and theoretical modeling. Table 2 shows typical values for both ε' and tanδ for general meteorite groups, while table 3 displays the permittivity of silicate minerals and organics.

Table 2
Typical permittivity (ε', tanδ) values for different asteroid and meteorite groups.

| Asteroid type | Meteorite group | Silicates | Phyllosilicates | Carbons | Metals | Density (kg $m^{-3}$) | ε | tan δ (max) |
|---|---|---|---|---|---|---|---|---|
| C | CR | 91.0% | 0.0% | 2.0% | 7.0% | 3230 ± 280 | 8.2 | 0.019 |
| | CM | 25.0% | 70.0% | 5.0% | 0.0% | 2710 ± 110 | 6.3 | 0.029 |
| | CI | 10.0% | 80.0% | 10.0% | 0.0% | 2120 ± 400 | 5.9 | 0.037 |
| S | H | 91.0% | 0.0% | 1.0% | 8.0% | 3640 ± 120 | 9.3 | 0.012 |
| | L | 95.0% | 0.0% | 1.0% | 4.0% | 3510 ± 110 | 8.3 | 0.012 |
| | LL | 97.0% | 0.0% | 1.0% | 2.0% | 3480 ± 80 | 7.8 | 0.012 |
| M | Mesosiderites | 25.0% | 0.0% | 0.0% | 75.0% | 4400 ± 300 | | |

Note. Meteorite group with the associated asteroid type: mineralogical model (volume fraction), density (from Britt and Consolmagno, 2003) and estimated permittivity based on Maxwell Garnet modeling. Direct observations of asteroid interior and regolith structure: Science measurement requirements (Herique et al. 2017).

Table 3
Permittivity of minerals and organics.

| | ε | tan δ | FREQUENCY | Porosity | REFERENCES |
|---|---|---|---|---|---|
| **SILICATES** | | | | | |
| *OLIVINE* | 7.1 | $4 \cdot 10^{-3}$ | 1 MHz | 0 | Olhoeft, 1979 |
| *OLIVINE* | 7.3 | $4 \cdot 10^{-2}$ | 1 MHz | 0 | Olhoeft, 1979 |
| *PYROXENES* | 7.9 | $8 \cdot 10^{-3}$ | 1 MHz | 0 | Olhoeft, 1979 |
| **PHYLLOSILICATES** | | | | | |
| *SERPENTINE* | *6.4 (6.4)* | *$4 \cdot 10^{-2}$ ($10^{-2}$)* | *35 (450) MHz* | | Campbell and Ulrichs (1969) |
| *SERPENTINE* | *6.4 (7.0)* | *$6 \cdot 10^{-2}$ ($2 \cdot 10^{-2}$)* | *35 (450) MHz* | | Campbell and Ulrichs (1969) |
| *MONTMORILLONITE* | *4.2–4.8* | | *90 MHz* | *<20%* | Herique et al. (2002) |
| **CARBON** | | | | | |
| *GRAPHITE* | *15–23* | *0.5–0.85* | *1–10 GHz* | *42%* | Hotta et al. (2011) |
| *PURE CARBON* | *23–30* | *0.35–0.4* | *1–10 GHz* | *37%* | Hotta et al. (2011) |
| *CARBON BLACK* | *6.0–9.0* | *0.4* | *1–10 GHz* | *12%* | Hotta et al. (2011) |
| *COAL with H – S – O – N* | *1.94–2.21* | *0.02–0.2* | *1–10 GHz* | *~50%* | Hotta et al. (2011) |
| **METAL** | | | | | |
| *HEMATITE + MAGNETITE* | 15.0 | 0.2 | 50 MHz | | Stillman and Olhoeft (2008) |

Note. Permittivity of relevant minerals and organics (from the literature; compilation of permittivity in Herique et al., 2016). Direct observations of asteroid interior and regolith structure: Science measurement requirements (Herique et al. 2017).

There are more options of internal structures to be examined and numerically modeled for various other bodies. Belton et al. in 2006, presented the layered pile model for comet 9P/Tempel 1 in which the authors suggest that the accretion process of Tempel 1 took place through layers, as basic structural elements, from the nuclei center and outwards. This model could also be applied in other comets like Gerasimenko. Moreover, as discussed in section 2.2, another interesting approach to Eros is the "heavily fractured" structure which can also be modeled possibly using highly anisotropic fields to represent the fractures in the asteroid and then applying material masks on top of that fracture field.

# References


Abell, P. A., Vilas, F., Jarvis, K. S., Gaffey, M. J., & Kelley, M. S. (2006). MINERALOGICAL COMPOSITION OF (25143) ITOKAWA 1998 SF36 FROM VISIBLE AND NEAR-INFRARED REFLECTANCE SPECTROSCOPY: EVIDENCE FOR PARTIAL MELTING. *Lunar and Planetary Science XXXVII*.

Belton, M. J., Thomas, P., Veverka, J., Schultz, P., A'Hearn, M. F., Feaga, L., . . . Kissel, J. (2006). The internal structure of Jupiter family cometary nuclei from Deep Impact observations: The "talps" or "layered pile" model. *Icarus 187 (2007) 332–344*.

Cheng, F. A. (2003). Implications of the NEAR mission for internal structure of Mathilde and Eros. *Advances in Space Research 33 (2004) 1558–1563*.

Cookson, C. (2017, October 19). *Space mining takes giant leap from sci-fi to reality*. Retrieved from Financial Times: https://www.ft.com/content/78e8cc84-7076-11e7-93ff-99f383b09ff9

Foley, C. N., Nittler, L. R., McCoy, T. J., Lim, L. F., Brown, M., Starr, R. D., & Trombka, J. I. (2006). Minor element evidence that Asteroid 433 Eros is a space-weathered ordinary chondrite parent body. *Icarus 184 (2006) 338–343*.

Fujiwara, A., Kawaguchi, J., Yeomans, D. K., Abe, M., Mukai, T., Okada, T., . . . Uesugi, K. (2006). The Rubble-Pile Asteroid Itokawa as Observed by Hayabusa. *Science VOL 312*.

Gaffey, M. J., Bell, F. J., Hamilton Brown, R., Burbine, T. H., Piatek, J. L., Reed, K. L., & Chaky, D. A. (1993). Mineralogical Variations within the S-type Asteroid Class. *Icarus 106, 573-602 (1993)*.

Grimm, R. E., David, S. E., Sava, P., & Ittharat, D. (2015). Radio reflection imaging of asteroid and comet interiors II: Results and recommendations. *Advances in Space Research 55 (2015) 2166–2176*.

Herique, A., Agnus, B., Asphaug, E., Barucci, A., Beck, P., Bellerose, J., . . . Zine, S. (2017). Direct observations of asteroid interior and regolith structure: Science measurement requirements. *Advances in Space Research xxx (2017) xxx–xxx*.

Holger Sierks, C. B. (2015). On the nucleus structure and activity of comet 67P/Churyumov-Gerasimenko. *Science VOL 347 ISSUE 6220*.

Kroese, D. P., & Botev, Z. I. (2015). Spacial Process Simulation. In V. Schmidt, *Stochastic Geometry, Spacial Statistics and Random Fields.* Springer.

Lowry, S. C., Weissman, P. R., Duddy, S. R., Rozitis, B., Fitzsimmons, A., Green, S. F., . . . Van Oers, P. (2014). The Internal Structure of Asteroid (25143) Itokawa as Revealed by Detection of YORP Spin-up. *Astronomy & Astrophysics, January 7, 2014*.

Massironi, M., Simioni, E., Marzari, F., Cremonese, G., Giacomini, L., Pajola, M., & ...& Preusker, F. (2015). Two independent and primitive envelopes of the bilobate nucleus of comet 67P. *Nature, 526(7573), 402*.

McSween Jr., H. Y. (1977). Petrographic variations among carbonaceous chondrites of the Vigarano type. *Geochimica et Cosmochimica Acta, 41(12), 1777-1790*.

Nakamura, T., Noguchi, T., Masahiko, T., Zolensky, M. E., Kimura, M., Tsuchiyama, A., . . . Kawaguchi, J. (2011). Itokawa Dust Particles: A Direct Link Between S-Type Asteroids and Ordinary Chondrites. *Science VOL 333*.

Pascale Ehrenfreund, Daniel P. Glavin, Oliver Botta, George Cooper, & Jeffrey L. Bada. (2001). Extraterrestrial amino acids in Orgueil and Ivuna: Tracing the parent body of CI type carbonaceous chondrites. *Proceedings of the National Academy of Sciences, 98 (5) 2138-2141; DOI: 10.1073/pnas.051502898*.

Quirico, E., Moroz, L. V., Beck, P., Schmitt, B., Arnold, G., Bonal, L., . . . Rosetta VIRTIS team. (2015). COMPOSITION OF COMET 67P/CHURYUMOV-GERASIMENKO REFRACTORY CRUST AS INFERRED FROM VIRTIS-M/ROSETTA SPECTRO-IMAGER. *46th Lunar and Planetary Science Conference.*

Reddy, V., Dunn, T. L., Thomas, C. A., Moskovitz, N. A., & Burbine, T. H. (2015). *Mineralogy and Surface Composition of Asteroids*. Retrieved from arxiv.org: https://arxiv.org/

Safaeinili, A., Gulkis, S., Hofstadter, M. D., & Jordan, R. L. (2010). Probing the interior of asteroids and comets using radio reflection tomography. *Meteoritics & Planetary Science 37. 1953 - 1963. 10.1111/j.1945-5100.2002.tb01176.x.* .

Sava, P., Ittharat, D., Grimm, R., & Stillman, D. (2015). Radio reflection imaging of asteroid and comet interiors I: Acquisition and imaging theory. *Advances in Space Research 55 (2015) 2149–2165*.

Van Schmus, W. R., & Wood, J. A. (1967). A chemical-petrologic classification for the chondritic meteorites. *Geochimica et Cosmochimica Acta. 31 (5): 747–765. Bibcode:1967GeCoA..31..747V. doi:10.1016/S0016-7037(67)80030-9.*

Weisberg, M., McCoy, T. J., & Krot, A. N. (2006). Systematics and Evaluation of Meteorite Classification.

Wilkison, S. L., Robinson, M. S., Thomas, P. C., Veverka, J., McCoy, T. J., Murchie, S. L., . . . Yeomans, D. K. (2002). An Estimate of Eros's Porosity and Implications for Internal Structure. *Icarus 155, 94–103, doi:10.1006/icar.2001.6751*.